

1 **Responses of field-aligned currents and equatorial electrojet to sudden decrease
2 of solar wind dynamic pressure during the March 2023 geomagnetic storm**

4 Guan Le¹, Guiping Liu¹, and Endawoke Yizengaw², Chin-Chun Wu³, Yihua Zheng¹, Sarah Vines^{4,5},
5 Natalia Buzulukova^{1,6}

7 ¹NASA Goddard Space Flight Center, Greenbelt, MD (guan.le@nasa.gov)

8 ²The Aerospace Corporation, El Segundo, CA

9 ³Naval Research Laboratory, Washington, DC

10 ⁴Applied Physics Laboratory, Laurel, MD

11 ⁵Now at Southwest Research Institute, San Antonio, TX

12 ⁶University of Maryland, College Park, MD

14 Corresponding author: Guan Le (guan.le@nasa.gov)

17 **Key Points:**

- 19 1. Direct evidence of prompt penetration of electric field in the equatorial ionosphere caused
20 by negative solar wind pressure pulse
- 22 2. Transient counter electrojet caused by westward penetration electric field after the arrival of
23 negative pressure pulse
- 25 3. Significant decrease of global large-scale FACs and transient enhancement of localized FAC
26 in response to negative pressure pulse

29 **Abstract**

30 We present the observations of field-aligned currents and the equatorial electrojet during the 23
31 March 2023 magnetic storm, focusing on the effect of the drastic decrease of the solar wind
32 dynamic pressure occurred during the main phase. Our observations show that the negative pressure
33 pulse had significant impact to the magnetosphere-ionosphere system. It weakened large-scale field-
34 aligned currents and paused the progression of the storm main phase for \sim 3 hrs. Due to the sudden
35 decrease of the plasma convection after the negative pressure pulse, the low-latitude ionosphere was
36 over-shielded and experienced a brief period of westward penetration electric field, which reversed
37 the direction of the equatorial electrojet. The counter electrojet was observed both in space and on
38 the ground. A transient, localized enhancement of downward field-aligned current was observed
39 near dawn, consistent with the mechanism for transmitting MHD disturbances from magnetosphere
40 to the ionosphere after the negative pressure pulse.

41

42 **Plain Language Summary**

43 The solar wind is a continuous stream of charged particles blowing from the Sun. The Earth's
44 magnetic field forms a protective shield around our planet, called the magnetosphere, which deflects
45 most of the solar wind particles away from the Earth. Disturbances in the solar wind can interact
46 with the magnetosphere and impact the Earth's upper atmosphere (ionosphere). The interaction
47 creates electric fields forcing charged particles to move in the magnetosphere, which creates electric
48 currents flowing along the magnetic field lines connecting to the high-latitude ionosphere and drives
49 the movement of charged particles there. The low-latitude ionosphere is generally shielded from
50 these electric fields. Sudden changes in the solar wind can break such balance, leading to the
51 electric field penetration to low latitudes. We examined how the magnetosphere and ionosphere
52 interacted during the 23 March 2023 geomagnetic storm, focusing on what happened when the solar
53 wind dynamic pressure suddenly decreased. We found the pressure drop caused a sudden decrease
54 of the high-latitude electric field, resulting in a brief period of overshielding and the electric field in
55 the equatorial ionosphere reversed its direction. This changed the direction of the equatorial
56 electrojet, a major electric current in the ionosphere at the magnetic equator.

57 **1 Introduction**

58

59 In steady-state conditions, the low-latitude ionosphere is shielded from the high-latitude convection
60 electric field due to the partial ring current-associated region-2 (R2) field-aligned currents (FACs)
61 which act to oppose the electric field associated with region-1 (R1) FACs (e.g., Southwood, 1977).
62 However, it can be directly coupled to the magnetospheric disturbances through prompt penetration
63 of the convection electric field during active times (Nishida, 1968; Jaggi and Wolf, 1973; Fejer et
64 al., 1979).

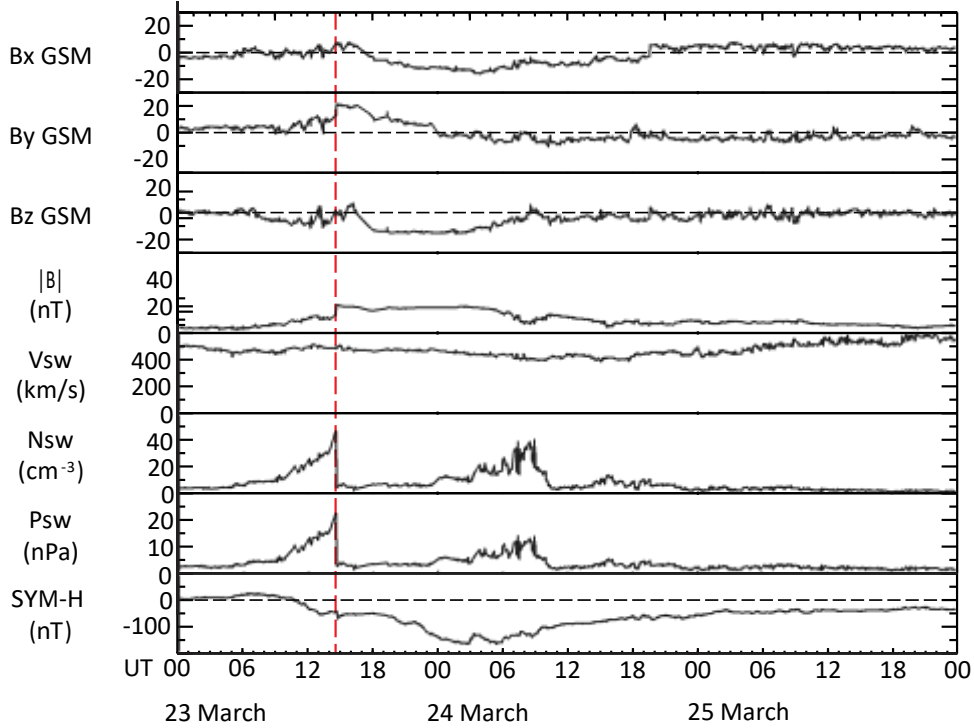
65

66 The equatorial electrojet (EEJ), an intense band of eastward electric current flowing along the
67 dayside magnetic equator in the E-region ionosphere (~ 110 km altitude), is driven by an eastward
68 zonal electric field from plasma-neutral collisional interactions known as the E-region wind dynamo
69 (Richmond, 1973; Heelis, 2004). The intensity and polarity of the EEJ respond directly to the
70 perturbations of the zonal electric field. Variations of the EEJ often serve as an indicator for the
71 equatorial zonal electric field perturbations, which can be caused by either neutral wind changes
72 from lower atmosphere forcing or prompt penetration electric fields (PPEFs) from enhanced
73 magnetosphere-ionosphere (M-I) coupling. Many studies have used EEJ variations to probe the
74 presence of PPEFs that are attributed to interplanetary magnetic field (IMF) variations (e.g.,
75 Yizengaw et al., 2011, 2016) or solar wind dynamic pressure pulses (e.g., Nilam et al., 2020, 2023).
76 Understanding the sources and the process of PPEFs continues to be a subject of ongoing
77 investigation (Kelley et al., 2003; Fejer et al., 2024).

78

79 This paper reports the observations of the M-I coupling and its effect on the equatorial ionosphere
80 in response to a sudden decrease of the solar wind dynamic pressure during the main phase of the
81 23 March 2023 geomagnetic storm. Figure 1 shows 1-min resolution OMNI data for the IMF and
82 solar wind parameters along with ground-based SYM-H index for 23-25 March 2023. This large
83 storm (minimum Dst ~ -170 nT, Kp ~ 7) was associated with the passage of an interplanetary
84 coronal mass ejection (ICME), triggered by the southward IMF in both the sheath and the ICME
85 regions. A drastic density decrease was observed at the boundary crossing from the sheath to the
86 ICME by the WIND spacecraft. As a result, a significant negative solar wind pressure pulse hit the

87 Earth's magnetosphere during the main phase of the storm (1440 UT, marked by the red dashed line
 88 in Figure 1). The solar wind density as well as the dynamic pressure decreased \sim 10 times.



90 Figure 1. The 1-min resolution OMNI data. The negative pressure pulse during the main phase of the storm is
 91 marked by the red dashed line.

92
93
94 We examine how FACs at high latitudes and the EEJ at the equator responded to the negative
95 pressure pulse using both space and ground-based magnetic field data. In the following sections, we
96 first present evidence for a transient PPEF associated with the pressure pulse from the ground based
97 EEJ observations. Then we examine the response of large-scale FACs globally by AMPERE and
98 locally by Swarm satellites. We also analyze the EEJ observations in space by Swarm, which
99 provide additional evidence for the transient PPEF associated with the pressure pulse. Finally, we
100 discuss the dynamic processes involving solar wind pressure pulse interacting with the
101 magnetosphere and coupling into the polar ionosphere, that allow us to understand the behaviors of
102 the equatorial ionosphere.

104 2 Observations

106 2.1 Ground-based Observations of EEJ

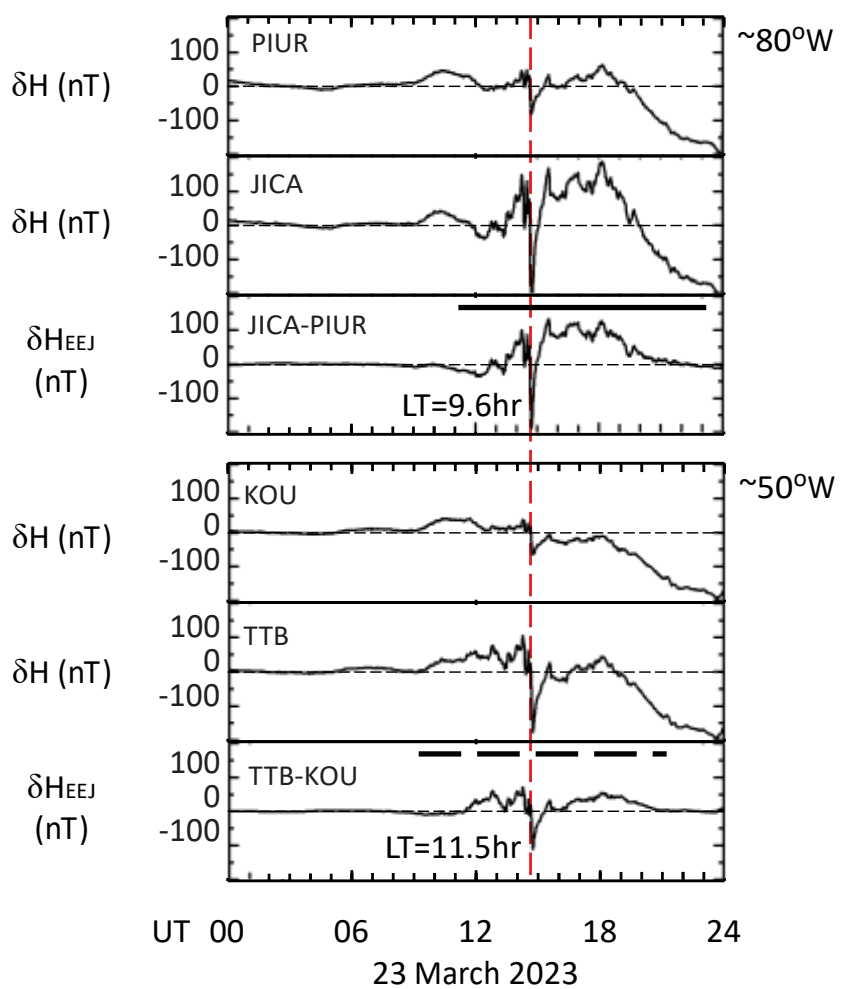
107
108 The EEJ signals can be obtained from a pair of ground magnetometer stations located near the
109 magnetic equator on the same meridian, one directly under the EEJ at the equator (within $\pm 3.5^\circ$) and
110 the other just off the EEJ region (6° – 9° from the magnetic equator) (Anderson et al., 2004;
111 Yizengaw et al., 2014). The EEJ signals centered at the magnetic equator extend over only a small
112 range of latitudes on either side because the EEJ current is confined in a narrow latitudinal band
113 (within $\pm 3^\circ$). But both stations are expected to record the same magnetic field variations from other
114 large-scale current sources, such as the solar quiet (Sq) currents, the ring current, and the
115 magnetopause current. The EEJ signals are extracted from the difference of the H-components
116 between the two stations. In this study, we used two pairs of geomagnetic observatories at two
117 meridians ($\sim 80^\circ$ W and $\sim 50^\circ$ W). One pair is located at Jicamarca (JICA, 11.95° S/ 76.87° W GEO,
118 MLat = 0.6° N) and Piura (PIUR, 5.2° S/ 80.6° W GEO, Mlat = 6.9° N) in Peru. The other pair is
119 located at Tatuoca, Brazil (TTB, 1.21° S/ 48.5° W GEO) and Kourou, French Guyana (KOU,
120 5.21° N/ 52.7° W GEO). The magnetic latitudes for TTB and KOU are 2.98° N and 10.72° N,
121 respectively, based on the model. However, they are within the region of South Atlantic Anomaly
122 with rapid northward moving of the magnetic equator, which passed the TTB in March 2013
123 (Morschhauser et al., 2017; Yizengaw, 2020). TTB should be slightly south of and KOU closer to
124 the magnetic equator than the model prediction today.

125
126 Figure 2 shows the magnetic fields from the 2 pairs of ground observatories on 23 March 2023 with
127 three subpanels for each pair, from top to bottom, showing the H-component with the background
128 removed (dH) off the magnetic equator, at the magnetic equator, and the EEJ signal (dH_{EEJ} , the
129 differences between dH at the geomagnetic equator and off the equator), respectively. The
130 horizontal bar in the 3rd subpanel indicates dayside hours (6–18 LT) at the equator station. The red
131 dashed line indicates the time of the negative pressure pulse (1440 UT) in Figure 1. The local time
132 (LT) of the pressure pulses at the two equator stations are also noted in Figure 2.

133
134 The eastward zonal electric field from the wind dynamo drives the eastward EEJ, producing a
135 positive magnetic field perturbation ($dH_{EEJ} > 0$) in the dayside. This is generally the case in Figure 2
136 except for a brief period immediately following the negative pressure pulse. There was a transient

137 negative impulse of the H-component at all the stations, consisting of a sharp decrease (~ 6 min) and
 138 a relatively gradual (~ 1 hour) return, apparently due to the sudden decrease of the magnetopause
 139 current and expansion of the magnetosphere in response to the negative pressure pulse (Araki and
 140 Nagano, 1988). However, the transient negative impulse at the equator station is much stronger than
 141 its off-equator counterpart, and the EEJ signature reversed its sign and minimized to -185 nT at
 142 80°W and -112 nT at 50°W, showing a transient counter electrojet flowing westward. This
 143 observation indicates the negative pressure pulse set up a transient westward electric field (~ 1 hour)
 144 in the equatorial ionosphere.

145



146

147 **Figure 2. Ground-based observations of the H-component from 2 pairs of ground observatories on 23 March**
 148 **2023, JICA-PIUR and TTB-KOU, respectively. The red dashed line marks the negative pressure pulse in Figure**
 149 **1. The black horizontal bars indicate the daytime (06-18 LT) at the equator stations.**

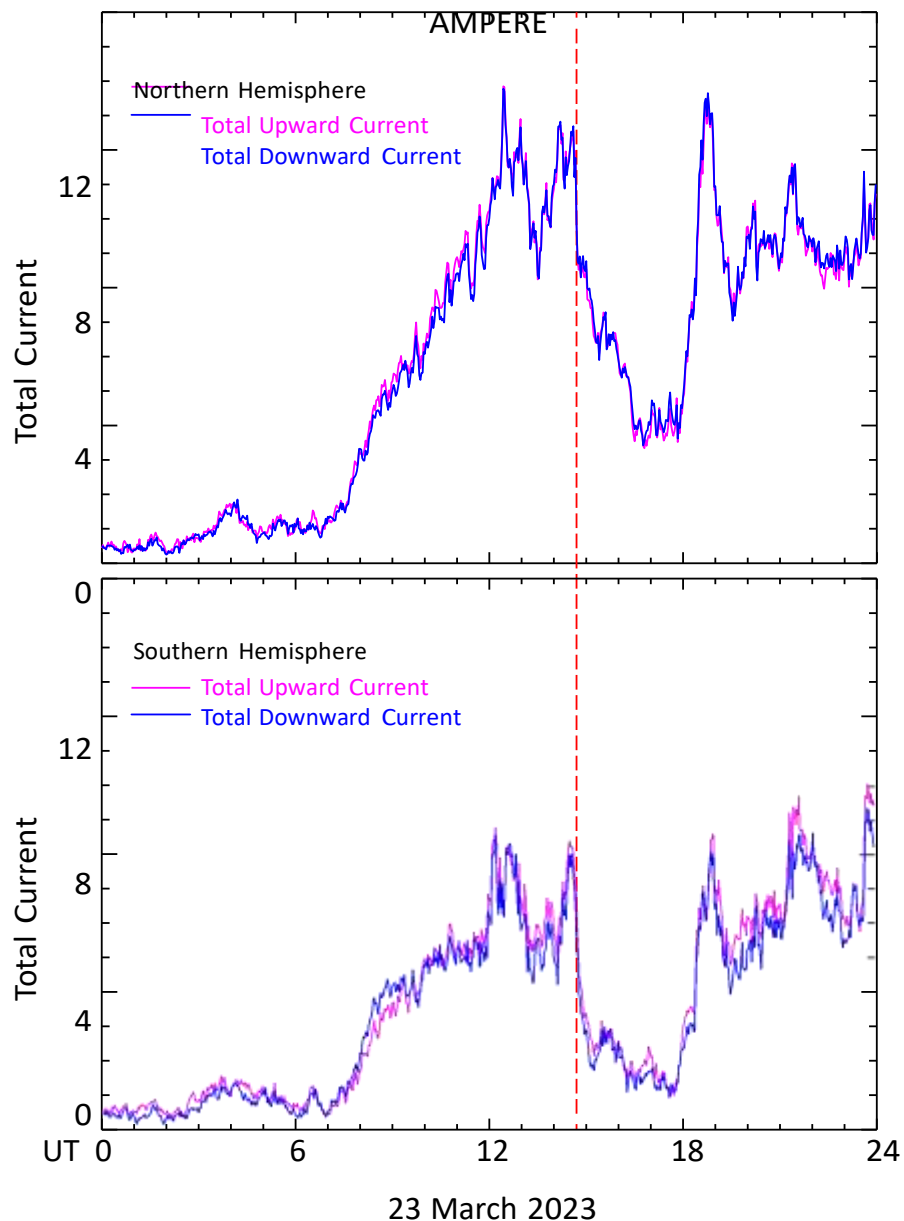
150

151
152 2.2 AMPERE Observations of Large-scale FACs
153
154 AMPERE observations of large-scale FACs are derived from measurements of magnetic field
155 perturbations from the Iridium constellation of more than 70 near-polar orbiting satellites [Anderson
156 et al., 2000]. It collects 10-min data to generate one global pattern of large-scale FAC distributions
157 and provides a continuous monitor of the state of the global M-I system. (AMPERE data will
158 unlikely reveal transient and localized variations due to the limitation of spatial and temporal
159 resolution.) Figure 3 shows the AMPERE observations of the total field-aligned currents flowing
160 into and out of the ionosphere on 23 March 2023 (Figure S1 provides the magnetic field
161 perturbations and global FAC maps). The total upward current out of one hemisphere is calculated
162 by integrating all the upward current density over the entire area above 40° latitude, and likewise for
163 the total downward current. Again, the red dashed vertical line corresponds to the negative pressure
164 pulse in Figure 1.
165
166 Starting from ~07 UT, the total FACs gradually intensified as the storm progressed with the SYM-
167 H index became more negative, representing an increasing active magnetosphere as FACs facilitate
168 the electromagnetic energy input from the magnetosphere into the ionosphere. There is a brief
169 period (~1 hr) of total current drop starting at ~13 UT, apparently associated with the northward
170 excursion of the IMF Bz component (Figure 1) which turned off the dayside reconnection and
171 reduced the magnetospheric convection temporally.
172
173 Figure 3 shows the total currents responded to the negative pressure in two stages. The total currents
174 dropped sharply at ~1440 UT due to the sudden sunward motion of the magnetopause and
175 expansion of the magnetosphere. The sudden reduction of the magnetopause current also caused a
176 step decrease of the SYM-H index (Figure 1). Then the total currents continued to decrease
177 gradually. The decreasing trend of the SYM-H index has flattened out within the storm main phase,
178 indicating the pause of the ring current development (Figure 1). This is expected as IMF Bz
179 fluctuated around zero and the expanded magnetosphere adjusted to the new state of reduced
180 geomagnetic activity level. At ~1630 UT, the IMF Bz gradually turned southward, which
181 terminated the decreasing trend of the total currents. At ~18 UT, both the total currents (Figure 3)

182 and the SYM-H index (Figure 1) showed that the magnetospheric activities began to intensify
183 rapidly with the prolonged steady southward IMF in the ICME. In summary of the AMPERE
184 observations, large-scale FACs were significantly weakened by the negative pressure pulse.

185

186



187

23 March 2023

188 **Figure 3. AMPERE Observations of the total upward and downward FACs in northern and southern**
189 **hemisphere, respectively.**

190

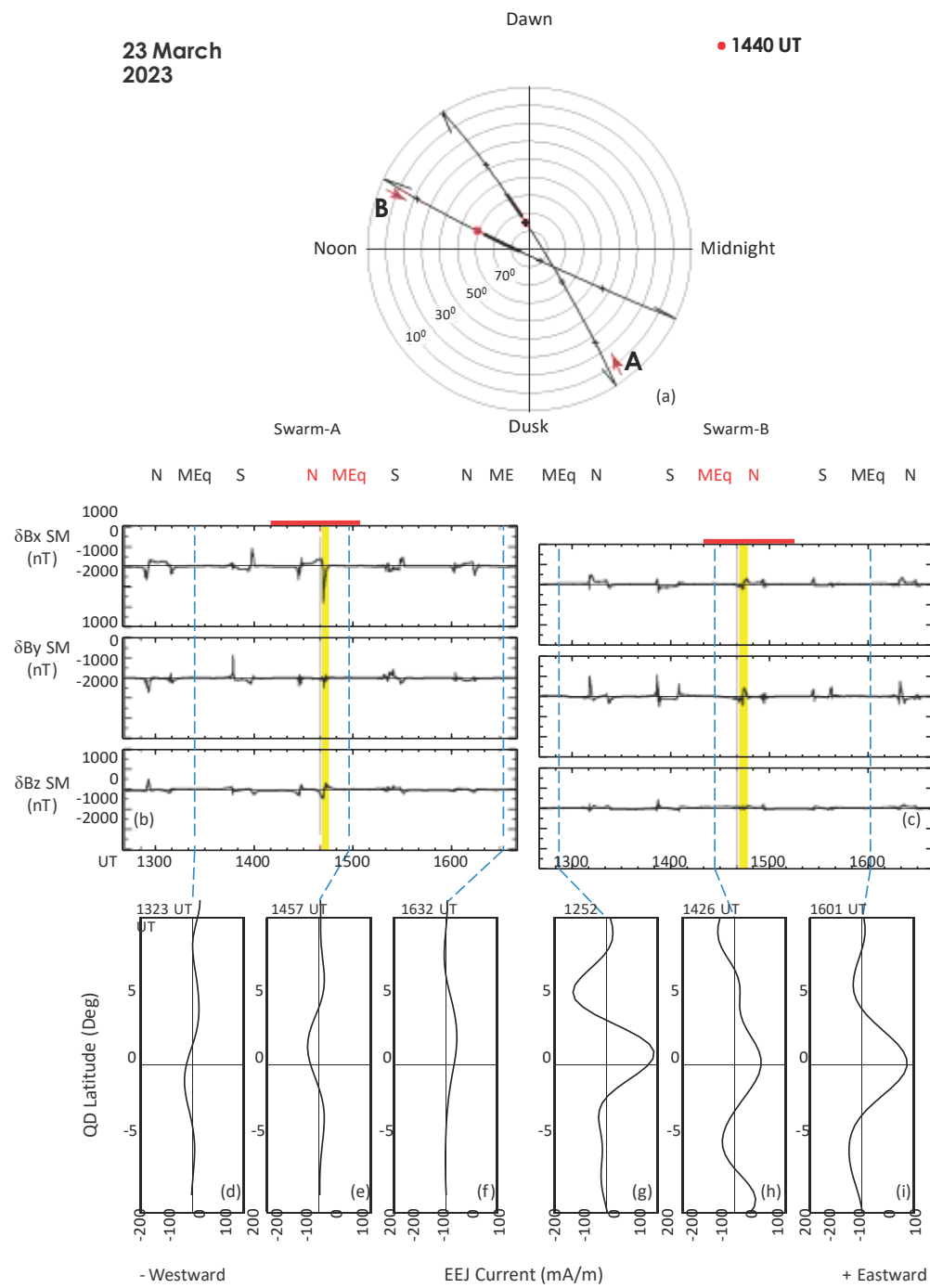
191
192 2.3 Swarm Observations of FACs and EEJ
193
194 Swarm is a three-satellite mission in a high-inclination (87.5°) low-Earth orbit, which provides
195 vector magnetic field data for frequent in situ measurements of FACs at high latitudes (Lühr et al.,
196 2015) and scalar magnetic field strength for the EEJ in the equatorial region (Alken et al., 2015).
197 Among the three satellites, A and C form a pair flying side by side at the same altitude (~ 460 km)
198 with a longitudinal separation of 1.4° . Swarm B has slightly higher altitude (~ 530 km) and its orbital
199 plane slowly drifts apart from those of Swarm A/C. In this study, we used two official Swarm level-
200 2 data products: (1) the vector magnetic field residuals \mathbf{dB} for the study of FACs, and (2) the height-
201 integrated latitudinal profile of eastward EEJ current. The EEJ current profile is estimated from the
202 Swarm scalar magnetic field measurements by isolating the EEJ signal from the many other
203 geomagnetic sources and then fitting the EEJ signal with a line current model (Alken et al., 2015).
204 The EEJ current peak at the magnetic equator provides a good estimate of the EEJ strength.
205
206 Figure 4 presents an overview of the Swarm observations. Figure 4a shows the spacecraft orbits for
207 the polar cap pass near 1440 UT, the intervals marked by the red bars in Figures 4b/4c. Figures 4b
208 and 4c contain 4 hours of Swarm vector magnetic field residuals \mathbf{dB} in solar magnetic (SM)
209 coordinate system centered at 1440 UT (red dashed line) for Swarm A and B, respectively. Swarm
210 C data are nearly the same as Swarm A (not shown). During this interval, Swarm made 5 passes of
211 the polar cap, denoted by N (S) for the northern (southern) hemisphere, and 3 crossings of the
212 dayside magnetic equator marked by MEq and the blue dashed lines. The perturbations in \mathbf{dB} are
213 the signals of FACs, occurring at auroral latitudes on both sides of the magnetic pole. The
214 latitudinal profiles of the estimated EEJ current at the dayside magnetic equator crossings are
215 presented in Figures 4d-4f for Swarm A and 4g-4i for Swarm B. The positive current is for eastward
216 EEJ.
217
218 Both Swarm A and B were in the dayside morning sector over the northern polar cap at the time of
219 the negative pressure pulse (red dots in Figure 4a). In Figure 4a, the tick marks on each trajectory
220 are separated by 10 min. The red arrows indicate the directions of the spacecraft motion. Swarm A

221 was moving from nightside to dayside and Swarm B from dayside to nightside with ~ 2 hr local
222 time separation of the orbital planes.

223
224 In Figures 4b&4c, the FACs observed before the negative pressure pulse were generally stronger
225 than those after at Swarm, in agreement with the AMPERE observations. The only exception is that
226 the FAC signal was significantly enhanced to ~ 2000 nT in magnitude shortly after the negative
227 pressure pulse at Swarm A (highlighted in yellow in Figure 4b) at ~ 7 LT (Figure 4a). The magnetic
228 field perturbations were mainly in the $-x$ direction (anti-sunward), which is the signature of a pair of
229 FACs flowing downward at higher and upward at lower latitudes, respectively. The enhanced FAC
230 pair had the same polarity of the regular R1/R2 FACs in the dawn sector. The enhanced dB_x
231 magnitude was mainly due to the much-enhanced downward FAC at higher latitudes since the
232 gradient (i.e., time rate of change) of dB_x was significantly higher at the poleward edge. The FACs
233 observed by Swarm B at nearly the same time (yellow-highlighted interval in Figure 4c) but at ~ 11
234 LT (Figure 4a) did not show the same feature, neither did the subsequent FACs in the pre-midnight
235 sector. When Swarm A returned to the same region in next orbit about 90 min later (~ 1615 UT),
236 the FACs have returned to the weakened state. These observations indicate the much-enhanced
237 downward FAC is a localized (near dawn) and transient (duration < 90 min) phenomenon in
238 response to the sudden decrease of the solar wind dynamic pressure. The AMPERE observations
239 did not capture such a localized transient response.
240

241 We now examine the EEJ profiles. As Swarm B is much closer to the local noon at the dayside
242 equator, the EEJ signal is expected to be much stronger at Swarm B than Swarm A. Before the
243 negative pressure pulse, the EEJ profile is not well defined at Swarm A (1323 UT, Figure 4d),
244 mostly likely due to a very weak EEJ in early morning. But closer to the local noon, Swarm B
245 detected the typical eastward EEJ profile at 1252 UT (Figure 4e) and 1426 UT (Figure 4f). Then
246 about 17 min after the negative pressure pulse, Swarm A observed a well-defined westward EEJ, or
247 counter electrojet (Figure 4e). The observed counter electrojet appeared to be a transient
248 phenomenon. The EEJ returned to nominal eastward direction in the next two profiles, 1601 UT at
249 Swarm B (Figure 4i) and 1632 UT at Swarm A (Figure 4f). These observations are in agreement
250 with the ground-based EEJ currents in Figure 2.
251

252



255

Fig magnetic field residuals; (d-i) the latitudinal profiles of the EEJ around the magnetic equator.
ure
4.
Swa
rm
A
and
B
obse
rvat
ions
of
FA
Cs
and
the
EEJ
: (a)
Spa
cecr
aft
traj
ecto
ries
nea
r
the
neg
ativ
e
pres
sure
puls
e;
(b-
c)
the
vect
or

260
261
262 **3 Discussion**
263

264 We summarize the observations presented above.

265 • The solar wind dynamic pressure decreased significantly at the boundary of the ICME that
266 caused the 23 March 2023 magnetic storm. The negative pressure pulse arrived at the Earth
267 at 1440 UT during the main phase of the storm and the IMF B_z fluctuated between
268 northward and southward (Figure 1).

269 • The total large-scale FAC currents flowing into and out of the ionosphere decreased
270 significantly soon after the arrival of the negative pressure pulse based (Figure 3). The
271 overall geomagnetic activity level in the magnetosphere was weakened for more than 3 hrs,
272 which paused the progression of the storm main phase. The activity level picked up again
273 only after the IMF B_z turned strongly southward for an extended period during the passage
274 of the ICME.

275 • Swarm A observed a significant enhancement of the downward FAC at the poleward edge
276 of the FAC region near dawn shortly after the negative pressure pulse, which appeared to be
277 localized and transient (Figure 4). Nearly simultaneous Swarm B observations closer to the
278 local noon showed weakened FACs, consistent with the AMPERE observations.

279 • A transient counter electrojet was observed both in space by Swarm A (Figure 4) and on the
280 ground (Figure 2) within minutes after the arrival of the negative pressure pulse. The counter
281 electrojet lasted for ~ 1 hr and then returned to its regular eastward direction. The observed
282 transient reversal of the EEJ to the westward direction suggests that the equatorial
283 ionosphere experienced a brief period of a westward electric field after the negative pressure
284 pulse.

285
286 These observations demonstrate the profound impact to the M-I system by the negative pressure
287 pulse. The observed counter electrojet indicates a transient westward electric field associated with
288 the negative pressure pulse penetrated to the equatorial ionosphere from over-shielding (Hori et al.,
289 2012; Fujita et al., 2012). The penetration electric field was much stronger in magnitude than the
290 background eastward electric field from the wind dynamo so that the overall zonal electric field was

291 reversed. Our observations indicated there was a sudden decrease of the dawn-to-dusk (eastward)
292 convection electric field as evident by the sudden decrease of the total FAC currents flowing into
293 and out of the polar ionosphere immediately after the negative pressure pulse (Figure 3). The total
294 FACs then gradually decrease with a time scale of hours. However, SYM-H, the ring current index,
295 was flatten out in the same period, indicating the ring current did not immediately respond to the
296 weakened convection electric field (Figure 1). The delayed response of the ring current reflects the
297 time scale for the M-I system to gradually adjust to the expanded state of the magnetosphere with
298 decreased level of plasma convection (Earle and Kelley, 1987). Thus, there was a short period
299 when the low-latitude ionosphere was over-shielded and experienced a dusk-to-dawn (westward)
300 electric field. Based on the duration of the counter-electrojet in the ground-based observations
301 (Figure 2), the response of the ring current-R2 FAC system was delayed for ~6 min, and it took ~ 1
302 hr for the M-I system to gradually adjust itself to the decreased plasma convection level and the
303 low-latitude ionosphere to return to be fully shielded.

304

305 To understand the transient responses and localized enhancement of FACs, it is necessary to review
306 the current understanding of the underlying physical process. The M-I system responds to a sudden
307 pressure pulse in two phases, including a preliminary impulse (PI) and a two-stage main impulse
308 (MI) (e.g., Tamao, 1964a&b; Araki, 1977; Araki and Allen, 1982). The PI is due to the propagation
309 and conversion of a compressional wave front launched from the magnetopause when the
310 magnetosphere is suddenly compressed or expanded. The PI is transient by nature because its driver
311 is the interaction between the pressure pulse and the magnetopause, which disappears in minutes
312 after the impulse front propagates away from the dayside.

313

314 Although more previous studies focused on sudden pressure increases than decreases, the basic
315 physics is the same. Based on Tamao's (1964a&b) pioneer work, Araki (1994) proposed a M-I
316 coupling PI model to explain the global observations after geomagnetic sudden commencements.
317 As illustrated in their Figure 12, the magnetopause moves inward and the dawn-to-dusk
318 magnetopause current increases when the solar wind dynamic pressure suddenly increases. A
319 compressional MHD wave is excited on the magnetopause, which propagates into the equatorial
320 magnetosphere. The solar wind-magnetosphere interaction as a dynamo generates an enhanced
321 dusk-to-dawn electric field at the magnetopause ($J \times E < 0$). A dusk-to-dawn electric field and

322 associated inertia electric current are induced inside the magnetosphere. The extra magnetopause
323 current and the inertia current would form a counterclockwise current loop. The compressional
324 wave will be converted into the transverse Alfvén wave due to the nonuniformity of the
325 magnetosphere (Tamao, 1964b; Southwood and Kivelson, 1990). When the compressional wave
326 front reaches the region where the Alfvén speed has a largest spatial gradient, converted Alfvén
327 waves are generated and propagate along the field lines with associated FACs. A pair of FACs will
328 be a part of the current loop, downward in the dusk side and upward in the dawn side. This process
329 happens in time scale of minutes. So, the pair of FACs exists transiently at lower latitudes than the
330 regular R1 currents with opposite polarity. A quantitative detail of the PI process is provided in the
331 MHD simulations by Fujita et al. (2003a&b, 2005), and the source region of the MHD wave mode
332 conversion for the generation of the transient FACs was found to be in the region of $6 < L < 7$
333 (Fujita et al., 2003a).

334

335 In the case of negative pressure pulses, the observations by Araki (1988) and simulations by Fujita
336 et al. (2004, 2012) showed that the magnetospheric and ionospheric signatures mostly mirror those
337 in pressure pulses. The negative pressure pulse causes the expansion of the magnetosphere and a
338 decrease of the magnetopause current. The PI is associated with a dawn-to-dusk transient dynamo
339 electric field at the magnetopause and induced electric field in the magnetosphere. The equatorial
340 current loop would be clockwise to effectively reduce the magnetic field strength in the
341 magnetosphere, and the pair of transient FACs would be downward in the dawnside and upward in
342 the duskside, in the same polarity of the regular R1 currents. The transient and localized
343 enhancement of the downward FAC observed by Swarm A near dawn (Figure 4) matches the
344 predicted polarity of the FACs. However, our observations differ in an important aspect from the
345 model prediction. The transient, localized FAC enhancement was observed at the poleward edge of
346 the FAC region, implying the source region was near the magnetopause, as in the earliest work of
347 Tamao (1964a). Further theoretical and numerical investigation is still needed to understand the
348 source region of the transient FACs during the PI. In addition, understanding the role of the ring
349 current/R2 FAC system to the undershielding/overshielding and its restoration is particularly needed
350 in future simulations.

351

352

4 Conclusions

353
354 A drastic decrease of the solar wind dynamic pressure occurred during main phase of the 23 March
355 2023 geomagnetic storm in association with the boundary between the ICME and its sheath. Our
356 observations show that the negative pressure pulse had significant impact to the M-I system. It
357 weakened the overall geomagnetic activities and plasma convection and paused the progression of
358 the storm main phase for ~ 3 hrs. Due to the sudden decrease of the dawn-to-dusk convection
359 electric field, there was a transient period when the low-latitude ionosphere was over-shielded and
360 experienced a brief period of dusk-to-dawn (westward) penetration electric field. The transient
361 westward penetration electric field reversed the direction of the equatorial electrojet, and the
362 counter electrojet was observed both in space and on the ground. The response of the ring current-
363 R2 FAC system was delayed for ~6 min, and it took ~ 1 hr for the M-I system to adjust itself to the
364 decreased plasma convection level until the low-latitude ionosphere was fully shielded again.
365 Although the overall large-scale FACs were weakened by the negative pressure pulse, a transient,
366 localized enhancement of downward FAC was observed near dawn, consistent with the mechanism
367 for transmitting MHD disturbances in the M-I coupling after the negative pressure pulse. But the
368 latitudinal location of the localized FAC enhancement differed from the model prediction, which
369 calls further investigation of the MI coupling in response to the pressure pulse.
370
371

372 **Acknowledgements**

373

374 GL thanks Lan Jian for helpful discussion. EY was partially supported by the AFOSR (FA9550-20-
375 1-0119) and NSF (AGS-1848730) grants. NB was partially supported by NASA Internal Scientist
376 Funding Model on Mesoscale Dynamics.
377

378
379

380 **Open Research**

381
382 The OMNI data are available at <https://omniweb.gsfc.nasa.gov>. The JICA and PIUR magnetometer
383 data are available at Yizengaw (2024). The KOU and TTB magnetometer data are available at
384 INTERMAGNET (www.intermagnet.org). The AMPERE data are available at
385 <https://ampere.jhuapl.edu>. The Swarm data are accessible at
386 <https://earth.esa.int/eogateway/missions/swarm/data>.

387

388

389

390 **References**

391

392 Alken, P., S. Maus, A. Chulliat, P. Vigneron, O. Sirol, and G. Hulot (2015), Swarm equatorial
393 electric field chain: First results, *Geophys. Res. Lett.*, 42, 673–680.

394 <https://doi.org/10.1002/2014GL062658>

395

396 Anderson, D., A. Anghel, J. Chau, and O. Veliz (2004), Daytime vertical $E \times B$ drift velocities
397 inferred from ground-based magnetometer observations at low latitudes, *Space Weather*, 2, S11001.

398 <https://doi.org/10.1029/2004SW000095>

399

400 Araki, T. (1977), Global structure of geomagnetic sudden commencements, *Planet. Space Sci.*, 25,
401 373. [https://doi.org/10.1016/0032-0633\(77\)90053-8](https://doi.org/10.1016/0032-0633(77)90053-8)

402

403 Araki, T. (1994). A physical model of the geomagnetic sudden commencement. *Geophysical
404 Monograph-American Geophysical Union*, 81, 183-183. <https://doi.org/10.1029/GM081p0183>

405

406 T. Araki, J. H. Allen (1982), Latitudinal reversal of polarization of the geomagnetic sudden
407 commencement, *J. Geophys. Res.*, 87, 5207– 5216. <https://doi.org/10.1029/JA087iA07p05207>

408

409 Araki, T. and H. Nagano (1988), Geomagnetic response to sudden expansions of the
410 magnetosphere, *J. Geophys. Res.*, 93, 3983–3988. <https://doi.org/10.1029/JA093iA05p03983>

411

412 Earle, G. D., and M. C. Kelley (1987), Spectral studies of the sources of ionospheric electric fields,
413 *J. Geophys. Res.*, 92(A1), 213–224. <https://doi.org/10.1029/JA092iA01p00213>

414

415 Fejer, B., C. Gonzales, D. Farley, M. Kelley, and R. Woodman (1979), Equatorial electric fields
416 during magnetically disturbed conditions 1. The effect of the interplanetary magnetic field, *J.
417 Geophys. Res.*, 84(A10), 5797–5802. <https://doi.org/10.1029/JA084iA10p05797>

418

419 Fejer BG, Laranja SR and Condor P (2024), Multi-process driven unusually large equatorial
420 perturbation electric fields during the April 2023 geomagnetic storm. *Front. Astron. Space Sci.*
421 11:1351735. <https://doi.org/10.3389/fspas.2024.1351735>

422

423 Fujita, S., T. Tanaka, T. Kikuchi, K. Fujimoto, K. Hosokawa, and M. Itonaga (2003a), A numerical
424 simulation of the geomagnetic sudden commencement: 1. Generation of the field-aligned current
425 associated with the preliminary impulse, *J. Geophys. Res.*, 108(A12), 1416.
426 <https://doi.org/10.1029/2002JA009407>

427

428 Fujita, S., T. Tanaka, T. Kikuchi, K. Fujimoto, and M. Itonaga (2003b), A numerical simulation of
429 the geomagnetic sudden commencement: 2. Plasma processes in the main impulse, *J. Geophys.*
430 *Res.*, 108(A12), 1417. <https://doi.org/10.1029/2002JA009763>

431

432 Fujita, S., T. Tanaka, T. Kikuchi, and S. Tsunomura (2004), A numerical simulation of a negative
433 sudden impulse, *Earth Planets Space*, 56, 463–472. <https://doi.org/10.1186/BF03352499>

434

435 Fujita, S., T. Tanaka, and T. Motoba (2005), A numerical simulation of the geomagnetic sudden
436 commencement: 3. A sudden commencement in the magnetosphere-ionosphere compound system,
437 *J. Geophys. Res.*, 110, A11203. <https://doi.org/10.1029/2005JA011055>

438

439 Fujita, S., H. Yamagishi, K. T. Murata, M. Den, and T. Tanaka (2012), A numerical simulation of a
440 negative solar wind impulse: Revisited, *J. Geophys. Res.*, 117, A09219.
441 <https://doi.org/10.1029/2012JA017526>

442

443 Heelis, R. A. (2004). Electrodynamics in the low and middle latitude ionosphere: A tutorial. *Journal*
444 *of Atmospheric and Solar-Terrestrial Physics*, 66(10), 825–
445 838. <https://doi.org/10.1016/j.jastp.2004.01.034>

446

447 Hori, T., A. Shinbori, N. Nishitani, T. Kikuchi, S. Fujita, T. Nagatsuma, O. Troshichev, K. Yumoto,
448 A. Moiseyev, and K. Seki (2012), Evolution of negative SI-induced ionospheric flows observed by

449 SuperDARN King Salmon HF radar, J. Geophys. Res., 117, A12223,
450 <https://doi.org/10.1029/2012JA018093>

451

452 Jaggi, R. K., and R. A. Wolf (1973), Self-consistent calculation of the motion of a sheet of ions in
453 the magnetosphere, J. Geophys. Res.; Space Physics, 78(16), 2852-2866.
454 <https://doi.org/10.1029/JA078i016p02852>

455

456 Kelley, M. C., J. J. Makela, J. L. Chau, and M. J. Nicolls (2003), Penetration of the solar wind
457 electric field into the magnetosphere/ionosphere system, Geophys. Res. Lett., 30, 1158.
458 <https://doi.org/10.1029/2002GL016321>

459

460 Morschhauser, A., Brando Soares, G., Haseloff, J., Bronkalla, O., Protásio, J., Pinheiro, K., and
461 Matzka, J. (2017): The magnetic observatory on Tatuoca, Belém, Brazil: history and recent
462 developments, Geosci. Instrum. Method. Data Syst., 6, 367–376. <https://doi.org/10.5194/gi-6-367-2017>

464

465 Nishida, A. (1968), Coherence of geomagnetic *DP* 2 fluctuations with interplanetary magnetic
466 variations, J. Geophys. Res.: Space Physics, 73, 5549-5559.
467 <https://doi.org/10.1029/JA073i017p05549>

468

469 Richmond, A. D. (1973). Equatorial electrojet-1. Development of a model including winds and
470 instabilities. *Journal of Atmospheric and Terrestrial Physics*, 35(6), 1083-
471 1103. [https://doi.org/10.1016/0021-9169\(73\)90007-x](https://doi.org/10.1016/0021-9169(73)90007-x)

472

473 Southwood, D. J. (1977), The role of hot plasma in magnetospheric convection, J. Geophys. Res.,
474 82(35), 5512–5520. <https://doi.org/10.1029/JA082i035p05512>

475

476 Southwood, D. J., and M. G. Kivelson (1990), The magnetohydrodynamic response of the
477 magnetospheric cavity to changes in solar wind pressure, J. Geophys. Res., 95, 2301–2309.
478 <https://doi.org/10.1029/JA095iA03p02301>

479

480 Tamao, T. (1964a), The structure of three-dimensional hydromagnetic waves in a uniform cold
481 plasma, *J. Geomagn. Geoelectr.*, 16, 89– 114, 1964a. <https://doi.org/10.5636/jgg.16.89>

482

483 Tamao, T. (1964b), A hydromagnetic interpretation of geomagnetic SSC*, *Rep. Ionos. Space Res.*
484 *Jpn.*, 18, 16– 31.

485

486 Yizengaw, E. (2020). The potential impacts of the erratic motion of dip equator and magnetic poles.
487 *Journal of Geophysical Research: Space Physics*, 125, e2020JA028129.
488 <https://doi.org/10.1029/2020JA028129>

489

490 Yizengaw, E. (2024). Geomagnetic field data at Jicamarca and Piura on 23 March 2023 [Dataset].
491 Zenodo. <https://doi.org/10.5281/zenodo.10823058>

492

493 Yizengaw, E., M. B. Moldwin, A. Mebrahtu, B. Damtie, E. Zesta, C. E. Valladares, and P. Doherty
494 (2011), Comparison of storm time equatorial ionospheric electrodynamics in the African and
495 American sectors, *Journal of Atmospheric and Solar-Terrestrial Physics*, 73, 156-163.
496 <https://doi.org/10.1016/j.jastp.2010.08.008>

497

498 Yizengaw, E., M. B. Moldwin, E. Zesta, C. M. Biouele, B. Damtie, A. Mebrahtu, B. Rabiu, C. F.
499 Valladares, and R. Stoneback (2014), The longitudinal variability of equatorial electrojet and
500 vertical drift velocity in the African and American sector, *Ann. Geophys.*, 32, 231–238.
501 <https://doi.org/10.5194/angeo-32-231-2014>

502

503 Yizengaw, E., Moldwin, M. B., Zesta, E., Magoun, M., Pradipta, R., Biouele, C. M., et al. (2016).
504 Response of the equatorial ionosphere to the geomagnetic DP 2 current system. *Geophysical*
505 *Research Letters*, 43(14), 7364–7372. <https://doi.org/10.1002/2016gl070090>